Biophysical Journal
Article

Biophysical Society

Hydrophobic and electrostatic interactions modulate protein escape at the ribosomal exit tunnel

Phuong Thuy Bui[1,2] and Trinh Xuan Hoang[3,4,*]
[1]Institute of Theoretical and Applied Research, Duy Tan University, Hanoi, Vietnam; [2]Faculty of Pharmacy, Duy Tan University, Da Nang, Vietnam; [3]Institute of Physics, Vietnam Academy of Science and Technology, Ba Dinh, Hanoi, Vietnam; and [4]Graduate University of Science and Technology, Vietnam Academy of Science and Technology, Cau Giay, Hanoi, Vietnam

ABSTRACT After translation, nascent proteins must escape the ribosomal exit tunnel to attain complete folding to their native states. This escape process also frees up the ribosome tunnel for a new translation job. In this study, we investigate the impacts of energetic interactions between the ribosomal exit tunnel and nascent proteins on the protein escape process by molecular dynamics simulations using partially coarse-grained models that incorporate hydrophobic and electrostatic interactions of the ribosome tunnel of *Haloarcula marismortui* with nascent proteins. We find that, in general, attractive interactions slow down the protein escape process, whereas repulsive interactions speed it up. For the small globular proteins considered, the median escape time correlates with both the number of hydrophobic residues, N_h, and the net charge, Q, of a nascent protein. A correlation coefficient exceeding 0.96 is found for the relation between the median escape time and a combined quantity of $N_h + 5.9Q$, suggesting that it is ~6 times more efficient to modulate the escape time by changing the total charge than the number of hydrophobic residues. The estimated median escape times are found in the submillisecond-to-millisecond range, indicating that the escape does not delay the ribosome recycling. For various types of the tunnel model, with and without hydrophobic and electrostatic interactions, the escape time distribution always follows a simple diffusion model that describes the escape process as a downhill drift of a Brownian particle, suggesting that nascent proteins escape along barrier-less pathways at the ribosome tunnel.

SIGNIFICANCE The post-translational escape of nascent proteins at the ribosomal exit tunnel is relevant to both nascent protein folding and the productivity of ribosomes because the escape facilitates folding and a too-slow escape or a kinetically trapped protein could jam the ribosome tunnel. Here, we show that the escape time depends on the protein's energetic interactions with the tunnel in a predictable way and that the protein escape process follows a simple diffusion mechanism.

INTRODUCTION

The ribosomal exit tunnel is the first structure nascent polypeptides interact with as they undergo elongation at ribosomes during translation. The tunnel, which starts from the peptidyl-transferase center (PTC), where amino acids are polymerized onto the growing nascent chain and spans across the ribosome's large subunit, is a passage all nascent proteins must traverse to exit the ribosome. Such passage not only helps to protect nascent chains from aggregation but is also known to be involved in the regulations of translation (1–4) and nascent protein folding (5–8). Nascent proteins fold co-translationally (6–8) while traversing the tunnel, and there is evidence that the folding starts inside the tunnel (9–11). The narrow geometry of the tunnel, of ~10–20 Å in diameter and 80–100 Å in length, however, limits the polypeptide conformations within the tunnel to simple secondary structures (12,13) and small tertiary motifs (14). Also, because of the tunnel's spatial constraints, at the end of the translation process, nascent proteins can be found only partially folded with their N-terminal part emerged from the tunnel, whereas the C-terminal part, composed by 20–40 amino acids (15), is still located inside the tunnel. As the last amino acid of a nascent protein is released from the PTC, the expected post-translational processes are the escape of the entire protein from the exit tunnel and its subsequent folding to the native state. In contrast to co-translational folding, which depends on factors

Submitted May 7, 2021, and accepted for publication September 15, 2021.
*Correspondence: hoang@iop.vast.vn
Editor: Robert Best.
https://doi.org/10.1016/j.bpj.2021.09.027

associated with the translation process, such as the vectorial nature of protein synthesis (6), the nonequilibrium effect of chain growth (16) and the translation rates (17–20), post-translational escape, and folding processes are more independent while they are still under the influence of the ribosome tunnel. Few studies have addressed these post-translational processes (21–24).

The ribosomal exit tunnel is not just an inert conduit for nascent chains but provides them a medium with complex interactions. The tunnel is highly porous (15) and also has narrow clefts for water molecules and ions that mediate protein and nucleic acid interactions in a tight environment (25,26). The modulated shape of the tunnel with a constriction site is significantly conserved across species with some variations (27), suggesting that an important role is played by the tunnel shape. The space inside the exit tunnel is a characteristic electrostatic environment, with the electrostatic potential varied from -8 mV near the PTC to -22 mV near the exit port (28). This electro-negative potential is mostly due to the domination of the negative charges of the ribosomal RNA. Ribosomal proteins protruding into the tunnel have more specific interactions with nascent chains, such as hydrophobic interaction. It has been shown that the tunnel's electrostatics modulate the translation rates (4), whereas certain hydrophobic surface inside the tunnel can promote the α-helix formation of a nascent transmembrane peptide (29).

In recent works (21–23), by using coarse-grained modeling and molecular dynamics simulations, we have shown the escape process is concomitant with the folding process, and these two processes promote each other leading to both an efficient escape and an improved folding efficiency (21). Our studies indicate that the protein escape at the ribosome tunnel is driven by the following: 1) an enthalpic force associated with the folding of the protein outside the tunnel, 2) an entropy gain as the chain emerges from the tunnel, and 3) the stochastic motion of a partially folded chain. Interestingly, all these factors can be effectively captured by a simple diffusion model (21,22) that describes the protein escape as diffusion of a Brownian particle in a linearly decreasing potential field, i.e., the particle is pulled by a constant force along the escape direction. This diffusion process was shown to depend on the relative length of a nascent protein to the tunnel length (22) and to the tunnel shape (23). Globular proteins, which have lengths of more than 50 residues, can escape efficiently at the ribosome tunnel (22), whereas very short proteins or peptides, such as the 29-residue zinc finger, may experience a much slower diffusion and kinetic trapping (23). It was estimated that the escape times of globular proteins are in the submillisecond timescale (23). This timescale is much shorter than the times needed by ribosomes to translate one codon (tens to hundreds of milliseconds); therefore, it would not lead to a jamming of the ribosome tunnel. These results were obtained in simplified models of the tunnel, either in the form of a smooth cylinder (21,22) or a real-shape atomistic model (23) for which, apart from the tunnel's excluded volume, there were no energetic interactions between the tunnel and the nascent proteins.

The purpose of this study is to investigate the effects of hydrophobic and electrostatic interactions of the tunnel with nascent protein on the protein escape process. In principle, these interactions should decrease or increase escape rates depending on whether they are attractive or repulsive; however, their combined effects are not easily foreseen. The questions we asked are whether they lead to a qualitative change of the escape process compared with that at the tunnel without energetic interactions and whether some quantitative assessments can be obtained for the effects of these interactions on the escape time. To pursue this purpose, we consider the ribosomal exit tunnel of *Haloarcula marismortui* and a number of small globular proteins as nascent proteins. Hydrophobic and electrostatic interactions between the tunnel and nascent proteins are effectively incorporated into partially coarse-grained models to be used in molecular dynamics simulations. In particular, our models consider all heavy atoms of the ribosomal RNA but only the alpha carbon (C_α) atoms for ribosomal and nascent proteins. A standard structure-based Gō-like model (30) is employed for the nascent proteins. Gō-like models have native-centric, smooth funnel-like landscapes (31) leading to rapid folding. These types of models have been widely used to study the folding dynamics, typically, of isolated proteins in solution, showing significant agreements to experiments (32–35). There have been indications that co-translational folding proceeds through compact, non-native conformations within the tunnel for certain proteins (9,10). A number of recent studies of co-translational folding (20,24) have employed corroborated models that are essentially Gō-like but include also features of knowledge-based potentials to take into account effects of the sequence and non-native interactions. In this study, with rather a focus on the escape process, we restrict ourselves to the fully structure-based Gō-like model, assuming that non-native interactions lead only to perturbations (36) of the results given by native interactions. Such assumption, of course, cannot be applied to nascent proteins that totally misfold at the ribosome. On the other hand, the hydrophobic and electrostatic interactions between nascent proteins and the ribosome tunnel considered here are sequence based and, although being simplified, reflect the generic properties of amino acids. Our study shows that these energetic interactions lead to certain changes in the escape time distribution that depend in a simple way on the number of hydrophobic residues and the total charge of a protein. Interestingly, the diffusion model, which has been successfully applied to the protein escape at the excluded volume tunnels, also works well for the tunnel with energetic interactions.

MATERIALS AND METHODS

Gō-like model

For the nascent proteins, we consider seven small globular proteins of length between 56 and 108 whose melting temperature T_m has been measured experimentally for the purpose of determining the energy parameter of the Gō-like model (see below). These proteins consist of the B1 domain of protein G (GB1) (37), the SH3 domain (SH3) (38), the Z domain of Staphylococcal protein A (39), chymotrypsin inhibitor 2 (CI2) (40), cold-shock protein (CSP) (41), ubiquitin (UBQ) (42), and barnase (43) (see Table S1 for the Protein Data Bank (PDB) codes, T_ms, and other properties of these proteins). T_ms are found in the range from 43.8°C for CSP to 95°C for UBQ. Native states of the proteins are shown in Fig. 1 (*bottom*).

The proteins are considered in the Gō-like model of Clementi et al. (30), which follows the early lattice model by Gō (44). The native contact map in the model is revised in this study to incorporate the atomic van der Waals (vdW) radii from Tsai et al. (45) for proteins. A native contact between two amino acids in a PDB structure is defined to be present if there are at least two atoms in those amino acids found within a cut-off distance equal to 1.244 times the sum of their vdW radii from each other (46). In the Gō-like model, amino acid residues are represented by their C_α atoms, and preferable energies are assigned only to native interactions. Particularly, the energy of a native contact between residue i and residue j is given by

$$V_{nat}(r_{ij}) = \varepsilon_1\left[5\left(\frac{r_{ij}^*}{r_{ij}}\right)^{12} - 6\left(\frac{r_{ij}^*}{r_{ij}}\right)^{10}\right], \qquad (1)$$

where ε_1 is the potential depth, r_{ij} is the distance between the residues in a given conformation, and r_{ij}^* is the corresponding distance in the native state.

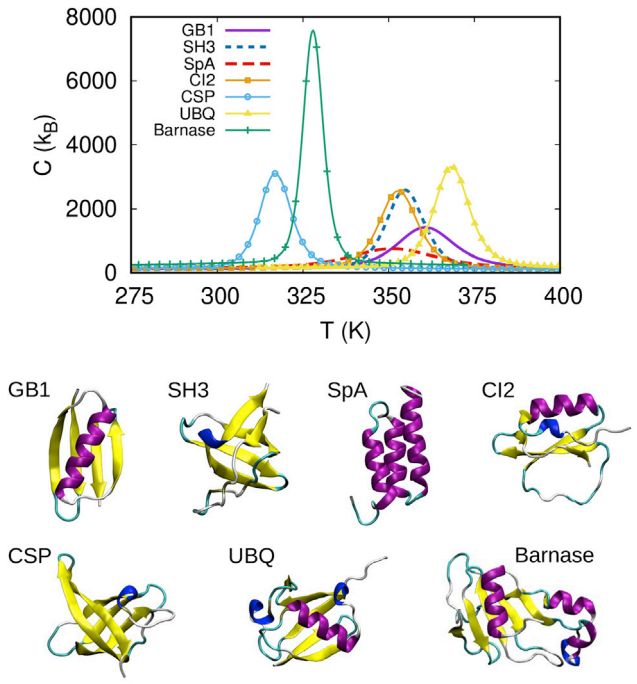

FIGURE 1 (*Top*) Temperature dependence of the specific heat of the proteins considered in this study. The specific heat was obtained by simulations in the Gō-like model with the energy parameter ε_1 calculated from the experimental melting temperature for each protein. (*Bottom*) Shown are the native states of the proteins considered. To see this figure in color, go online.

The energy parameter ε_1 in the Gō-like model represents an average energy contribution per contact from all native contacts in a protein's native state. One way to get an estimate of ε_1 is to match the folding temperature T_f, defined as temperature of the peak of the specific heat peak obtained in the Gō-like model, to the experimental melting temperature T_m taken from the literature. We have used this matching to determine ε_1 for all proteins considered (see Table S1). For each protein, T_f was obtained by molecular dynamics simulations without the tunnel and by using the weighted histogram technique (47,48) in calculating the specific heat. We find that ε_1 depends on the protein and varies in the range from 0.67 to 0.8 kcal/mol. The determination of ε_1 allowed us to get quantitative results at temperatures in real units. Fig. 1 (*top*) shows that at the temperature of 300 K, the specific heats of the proteins considered have relatively low values, indicating that the proteins are thermodynamically stable at this temperature.

Tunnel model

The model of ribosomal exit tunnel considered in this study is built on the atomistic tunnel model from previous work (23) and is based on the resolved structure of the large ribosome subunit of *H. marismortui* from the PDB with the PDB code 1jj2 (49). The model is not an all-atom one but is somewhat simplified by considering all heavy atoms of the ribosomal RNA but only the C_αs of the ribosomal proteins. To accelerate calculations, only ribosomal atoms within 30 Å from a predefined tunnel axis are included in the model, and they are kept fixed during the simulations. Depending on the interactions between the tunnel and nascent proteins, we consider three types of tunnel model, denoted as T1, T2 and T3, with the following definitions: the T1 model entails only excluded volume interaction, the T2 model includes the excluded volume interaction and the hydrophobic interaction, and the T3 model has additionally the electrostatic interaction on top of the excluded volume and the hydrophobic ones. These interactions are considered only between the tunnel and nascent proteins and are given as follows.

Excluded volume interaction

The excluded volume interaction is given between an amino acid residue a of a nascent protein with a heavy atom b of the ribosome in the form of a repulsive potential

$$V_{ex}(r) = \varepsilon_2\left(\frac{R_a + R_b + R_+}{r}\right)^{12}, \qquad (2)$$

where $\varepsilon_2 = 1.2$ kcal/mol, r is the distance between the two atoms, $R_a = 2.5$ Å is an effective radius of amino acid assumed to be the same for all amino acids, R_b is the vdW radius of the ribosomal atom, which depends on the atom's type (1.7 Å for carbon, 1.55 Å for nitrogen, 1.52 Å for oxygen, and 1.8 Å for sulfur and phosphorus), and $R_+ = 0.8$ Å is an additive radius (23) included as a compensation for the absence of hydrogen atoms in the model.

Hydrophobic interaction

Hydrophobic residues (Ile, Leu, Phe, Met, Val, Pro, and Trp) of a nascent chain interact with hydrophobic residues of ribosomal proteins via the 10–12 Lennard-Jones potential

$$V_{hp}(r) = \varepsilon_3\left[5\left(\frac{\sigma}{r}\right)^{12} - 6\left(\frac{\sigma}{r}\right)^{10}\right], \qquad (3)$$

where $\sigma = 5$ Å is an effective diameter of amino acids and ε_3 is the potential depth assumed to be constant for all pairs of hydrophobic residues and for

all proteins. Experimental studies (50,51) show that the energy contribution of a buried hydrophobic side chain to the protein stability is from 0.4 to 4.4 kcal/mol, depending on the side chain's type and the degree of its buriedness. If the average number of contacts per hydrophobic side chain is two, then a contact contributes an energy of 0.2–2.2 kcal/mol. In this work, we choose $\varepsilon_3 = 1.5$ kcal/mol, the supposed mean value of hydrophobic contact energies within this range.

Electrostatic interaction

In the ribosomal RNA, phosphorus atoms are assigned charges of $q = -1e$. In ribosomal and nascent proteins, the charges are assigned to the C_α atoms of the charged residues. Lysine and arginine residues are assigned charges of $q = +1e$, and glutamine and aspartate residues are assigned charges of $q = -1e$. All other amino acid residues have a zero charge. The electrostatic interaction is treated with a screened potential from the Debye-Hückel theory,

$$V_{el}(r) = \frac{1}{4\pi\varepsilon_0\varepsilon_r}\frac{q_i q_j}{r}\, e^{-r/\lambda_D}, \tag{4}$$

where r is the distance between the charges q_i and q_j of atoms i and j, respectively, ε_0 is the vacuum permittivity, the Debye's screening length $\lambda_D = 10$ Å, and the relative dielectric constant $\varepsilon_r = 78.5$.

Simulation method

Nascent chains were simulated by using a molecular dynamics method based on the Langevin equation of motion and a Verlet algorithm (21). All amino acids are assumed to have the same mass, m, and the same friction coefficient ζ. We adopt a unit system such that the mass unit is m, the length unit is σ, and the energy unit is kilocalorie per mole. Given that $m = 120$ g/mol and $\sigma = 5$ Å, the simulation time is measured in the reduced units of $\tau = \sqrt{m\sigma^2/(\text{kcal/mol})} \approx 3$ ps. The diffusion constants of amino acids in water at room temperature are varied between 5.8 and 8.1×10^{-10} m^2 s^{-1} (52), corresponding to an average friction coefficient $\zeta_{\text{water}} \approx 6 \times 10^{-9}$ g s^{-1}. The friction coefficient used in the simulations in this study is $\zeta = \zeta_{\text{sim}} = 1\sqrt{m\sigma^{-2}(\text{kcal/mol})} \approx 6 \times 10^{-11}$ g s^{-1} $\approx 0.01\zeta_{\text{water}}$. In the Gō-like model, the folding time (53) as well as the escape time (23) increase linearly with ζ in the overdamped regime (54); hence, the simulation time at $\zeta = \zeta_{\text{water}}$ can be obtained as 100 times larger than that at $\zeta = \zeta_{\text{sim}}$. At the water value of ζ, it has been suggested that the reduced time unit is $\tau_H \approx 3$ ns because of the irrelevance of the inertial terms in the Langevin equation (55). One can apply both the time rescaling due to the enlarged friction and the high-friction value of the reduced time unit to map the simulation time to real time (54,55). For example, a simulation time of 333τ obtained at $\zeta = \zeta_{\text{sim}}$ would correspond to 0.1 ms at realistic friction. It is useful to compare the simulation timescale with experiments. We have checked that the median folding time of GB1 obtained in the same Gō-like model at 298 K is 340τ, whereas the reported experimental refolding time of GB1 is ~1 ms (37), showing that the predicted folding time by simulations is ~10 times smaller than the experimental value. This ratio may not be the same for the escape time of GB1 as well as for other proteins because it depends on the reliability of the Gō-like model in reproducing the folding dynamics in vitro. We take this comparison, however, as a reference for assessing the estimates of the escape times.

Each simulation starts with one amino acid, the N-terminal residue of a protein, bound to the PTC. The nascent chain then is elongated from the PTC at a constant rate, with the typical growth time $t_g = 400\tau$ per residue. When the elongation is completed, the C-terminal residue is released from the PTC. The simulation is continued until the nascent protein has fully escaped the tunnel and folded. A protein is said to be fully escaped if all of its residues are found outside the tunnel region, which is set to be a cylinder of length $L = 72$ Å and radius of 15 Å centered along the tunnel axis (23). Here, L is the tunnel length and corresponds to the distance from the opening of the tunnel near the PTC to an inner edge of the tunnel exit port. A protein is said to be folded if the fraction of the number of native contacts is larger than 0.9 and the root mean squared deviation to the native state is smaller than 1.5 Å. Both the escape time and the folding time are measured from the moment of complete elongation. The statistics on the escape time and the folding time are typically drawn from 1024 independent simulations for each protein. For simplicity, we consider the escape and folding processes at the single temperature, $T = 298$ K, which represents a physiological condition.

We also employed the umbrella sampling technique (56) in equilibrium simulations with restraint potentials on the C-terminal residue (21) and the weighted histogram analysis method (47,48) to calculate the free energy of nascent protein as a function of the number of escaped residues,

$$F(N_{\text{out}}) = -k_B T \log P(N_{\text{out}}), \tag{5}$$

where $P(N_{\text{out}})$ is the probability of observing conformations having the number of escaped residues N_{out} obtained from the reweighted histograms.

Diffusion model

The diffusion model (22) considers the protein escape process as the diffusion of a Brownian particle in a potential field $U(x)$. Such process is governed by the Smoluchowski equation (57)

$$\frac{\partial}{\partial t}\, p(x,t) = \frac{\partial}{\partial x} D\left(\beta\frac{\partial U(x)}{\partial x} + \frac{\partial}{\partial x}\right) p(x,t), \tag{6}$$

where $p(x, t)$ is a probability density of finding the particle at position x and at time $t > 0$, given that it was found at position $x = 0$ at time $t = 0$; D is the diffusion constant, assumed to be position independent; and $\beta = (k_B T)^{-1}$ is the inverse temperature. The escape time is described as the first passage time of the particle reaching a distance L from an origin in the drift direction. Here, L corresponds to the length of the ribosome tunnel. Given the potential of the linear form $U(x) = -kx$, where k is the constant force acting on the particle and an absorbing boundary condition at $x = L$, the distribution of the escape time can be obtained via an exact solution (58) and is given by (22)

$$g(t) = \frac{L}{\sqrt{4\pi D t^3}}\exp\left[-\frac{(L - D\beta k t)^2}{4Dt}\right]. \tag{7}$$

Using the distribution in Eq. 7 one obtains the mean escape time

$$\mu_t \equiv \langle t\rangle = \int_0^\infty t\, g(t)\, dt = \frac{L}{D\beta k}, \tag{8}$$

with $D\beta k$ representing the mean diffusion speed and the standard deviation

$$\sigma_t \equiv \sqrt{\langle t^2\rangle - \langle t\rangle^2} = \frac{\sqrt{2L}}{D(\beta k)^{\frac{3}{2}}}. \tag{9}$$

Note that both μ_t and σ_t diverges when $k = 0$, for which $g(t)$ becomes a heavy-tailed Lévy distribution. It has been shown that D and βk depend on L, on the protein, and on other conditions such as the crowders' volume fraction outside the tunnel (22).

RESULTS AND DISCUSSION

Effect of translation rate on protein escape

The translation rate is known as a factor impacting co-translational folding—changing this rate, either globally (17) or locally (18,19), can coordinate the folding efficiency. These results indicate that co-translational folding is a history-dependent process, despite the fact that real translation rates in cells are relatively slow (5–20 amino acids per second). Because co-translational folding is followed by the escape process, it is expected that the translation rate also affects the protein escape at the ribosome tunnel. Within the Gō-like model and a cylinder tunnel, we have shown (21) that the distribution of fully elongated protein conformations has converged properties in terms of the number of native contacts and the radius of gyration if the protein elongation rate is sufficiently slow, such that the growth time per amino acid is of the order the folding time of an isolated protein in solution. For a real-shape tunnel with only excluded volume interaction (23), one finds an increased probability of kinetic trapping of the protein inside the tunnel compared with the smooth cylinder tunnel. The trapping probability also increases on decreasing the temperature.

In this study, to assess the effect of the translation rate on the protein escape at the ribosome tunnel with hydrophobic and electrostatic interactions, we carried out simulations for protein GB1 at the T3 tunnel with various growth times per amino acid t_g in the range from 200τ to 1200τ. Although most of the trajectories resulted in a successful escape and folding (see Fig. 2, *A–C* for examples of protein conformations), some fraction of trajectories ended with trapped conformations (Fig. 2, *D* and *E*). A trapped protein would require a much longer time, typically orders of magnitude longer than the average escape time in typical trajectories, to escape the tunnel. Fig. 3 shows that the dependences of the escape probabilities P_{escape} on time for various t_g have similar sigmoidal shapes and are different only at large times when the probabilities reach different saturation levels. For example, at the time of 1500τ, which is the time cut-off in the figure, the escape probability increases from ~93% to more than 99% as t_g increases from 200τ to 1200τ. Beyond that time cut-off, the escape probability continues to increase slowly with time; for example, for $t_g = 200\tau$, it reaches 95.2% after $10{,}000\tau$. Note that the trapping probability is equal to $1 - P_{\text{escape}}$ at a large time and, thus, is between 1 and 7%, depending on the value of t_g. It is shown that the slower the translation rate the smaller the probability of kinetic trapping in the escape process. Fig. 3 also shows that changing t_g only slightly affects the median escape time, t_{esc}, which corresponds to the midpoint of the curve, at which the escape probability is equal to 1/2.

The slowest translation speed in our simulations corresponds to the growth time per amino acid $t_g = 1200\tau \approx 3.6$ ms if the simulation time is compared to the experimental folding time of GB1 (see Materials and methods). This translation speed is at least an order of magnitude faster than real translation rates, suggesting that the trapping probability can be vanishingly small for GB1 at a realistic translation rate. This conclusion, however, should be taken with reservation to the approximations in our models, such as the C_α-only representation for proteins. It was shown that inclusion of amino acid side chains in the ribosomal proteins of the excluded volume tunnel model increases the trapping probability from 0 to 5%, and this probability also decreases with the growth time (23). In fact, the problem of kinetic trapping is considerable only for GB1, which is the smallest

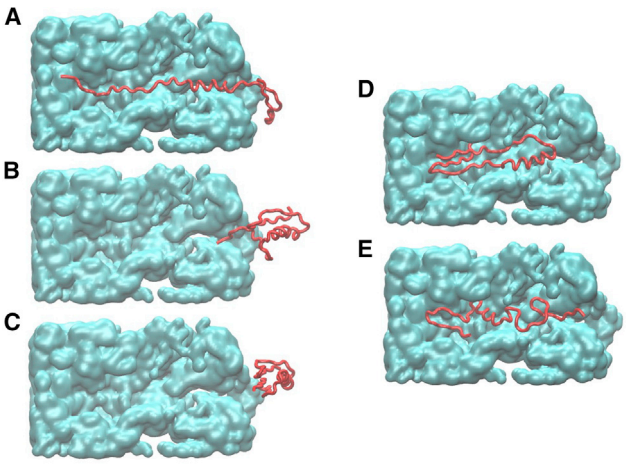

FIGURE 2 Examples of nascent protein conformations at the ribosomal exit tunnel. The tunnel (*cyan*) is shown from a cross section at the tunnel axis. The conformations (*red*), obtained by simulations for protein GB1 at the T3 tunnel model, show the protein being fully elongated at the tunnel (*A*), fully escaped from the tunnel (*B*), and completely folded outside the tunnel (*C*), from a typical trajectory. Some trajectories result in kinetically trapped conformations (*D* and *E*), which are fully fitted inside the tunnel. To see this figure in color, go online.

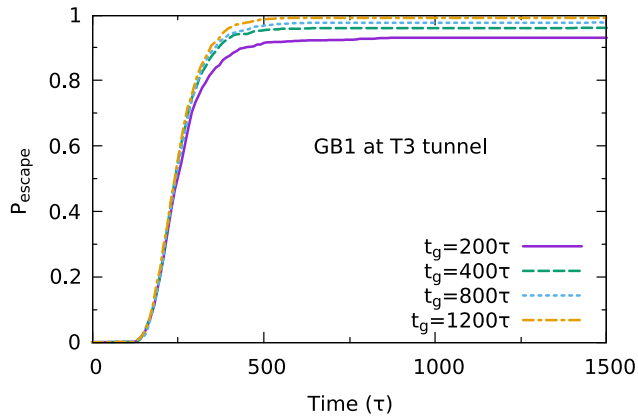

FIGURE 3 The escape probability P_{escape} as a function of time of protein GB1 at the T3 tunnel obtained with various growth time t_g per amino acid as indicated at $T = 298$ K. The time for calculating the escape probability is measured from the moment the protein's C-terminal residue is released from the PTC. To see this figure in color, go online.

proteins among the seven proteins considered. All other proteins were able to escape the tunnel with 100% successiveness within the simulation time cut-offs of few thousands of τ. Smaller proteins are more prone to kinetic trapping because they can fit inside the tunnel (23).

Effects of tunnel interactions

To figure out the effects of tunnel interactions on the escape process of nascent proteins, we compare the escape times and the escape probabilities for three types of the tunnel model, namely the T1, T2, and T3 models, as given in the Materials and methods. It is convenient to remind here that the T1 model considers only the excluded volume interaction between the tunnel and nascent proteins, the T2 model includes the excluded volume and the hydrophobic interactions, and the T3 model has the electrostatic interaction on top of the last two interactions. To save the simulation time in the following, we considered only the protein elongations with $t_g = 400\tau$.

Fig. 4 shows that for protein GB1, the escape time distribution at the T2 tunnel (Fig. 4 *B*) is shifted toward greater times and is more expanded than the one at the T1 tunnel (Fig. 4 *A*). The escape time distribution at the T3 tunnel (Fig. 4 *C*) is shifted toward smaller times and is narrower than the one at the T2 tunnel. These shifts can be understood as simply due to whether a given tunnel's interaction provides an overall attraction or repulsion with a nascent protein—an attraction would slow down the escape process, whereas a repulsion would speed it up. The hydrophobic interaction is always attractive and therefore leads to longer protein escape times. The electrostatic interaction entails both repulsion and attraction, depending on the protein's charges. GB1 protein has six positive charges and 10 negative charges (Table S1) and, given that the ribosome tunnel has an electro-negative potential, the overall electrostatic interaction of GB1 with the tunnel is repulsive and therefore makes the protein escape faster. Fig. 4, *D* and *E* shows that hydrophobic interaction leads to a slower increase of the escape probability with time and an increased probability of kinetic trapping. Specifically, at the time of 1500τ, the escape probability reaches 100% at the T1 tunnel (Fig. 4 *D*) but only ~96% at the T2 tunnel (Fig. 4 *E*), meaning that the probability of kinetic trapping has increased from 0% at the T1 tunnel to ~4% at the T2 tunnel. The electrostatic interaction in the T3 tunnel makes the escape probability increased faster with time (Fig. 4 *F*) but does not help the protein to avoid kinetic traps—the escape probability approximately reaches the same value at large times as at the T2 tunnel.

Fig. 5 shows that for protein SH3, the effect of hydrophobic interaction on the escape time distribution is the same as for protein GB1, whereas the effect of electrostatic interaction is different from that for GB1. One always sees a shift toward larger times for the escape time distribution by changing the tunnel type from T1 (Fig. 5 *A*) to T2 (Fig. 5

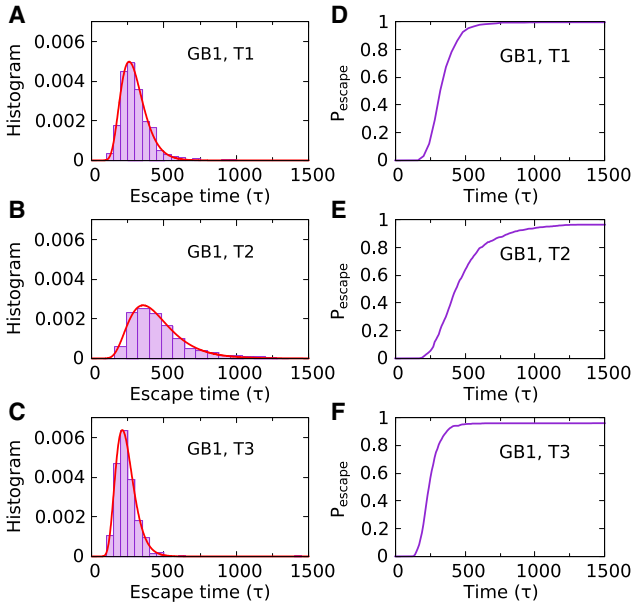

FIGURE 4 Distributions of the escape time (*A–C*) and the time dependences of the escape probability P_{escape} (*D–F*) of protein GB1 for the three types of tunnel model for the interactions between the tunnel and nascent proteins: the T1 tunnel with only excluded volume interaction (*A* and *D*), the T2 tunnel with excluded volume and hydrophobic interactions (*B* and *E*) and the T3 tunnel with excluded volume, hydrophobic, and electrostatic interactions (*C* and *F*). The data are obtained at $T = 298$ K and with $t_g = 400\tau$. To see this figure in color, go online.

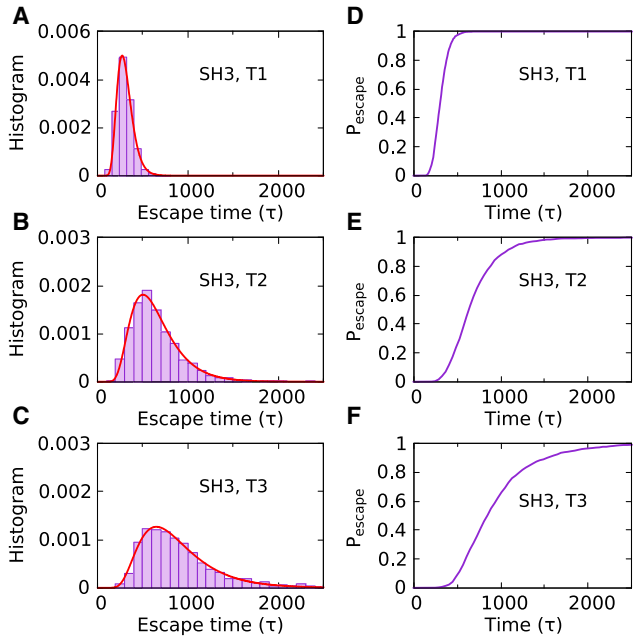

FIGURE 5 Distributions of the escape time (*A–C*) and the time dependences of the escape probability P_{escape} (*D–F*) for protein SH3 at the three types of the tunnel model as in Fig. 4. The data are obtained at $T = 298$ K and with $t_g = 400\tau$. To see this figure in color, go online.

B) or from T2 to T3 (Fig. 5 *C*). Like for GB1, the effects of tunnel's interactions can be also understood in terms of the overall attraction and repulsion. In contrast to GB1, the SH3 protein has more positive charges than negative charges (10 vs. 9) (Table S1); therefore, the overall electrostatic interaction of SH3 with the tunnel is attractive, leading to a slower escape. Note that both the hydrophobic and electrostatic interactions slow down the escape process but do not reduce the escape efficiency of SH3 protein. For this protein, the escape probability always reaches 100% at sufficiently large times without indication of kinetic trapping (Fig. 5, *D–F*). Thus, the impacts of energetic interactions on the escape time as well as on the kinetic trapping at the exit tunnel are protein dependent.

For five other proteins, the escape time distribution and the time dependence of the escape probability have the shapes that are qualitatively similar to those obtained for GB1 and SH3 (see Fig. S1). The distributions are different only by the position of the peak and the range of the escape time, which depend on the protein. Unlike GB1, the escape probabilities of all other proteins can reach 100% after certain times of few thousands of τ, indicating that kinetic trapping is not an issue for most proteins even in the presence of hydrophobic and electrostatic interactions with the tunnel.

To further evaluate the effects of tunnel interactions on the protein escape, we study the dependence of the median escape time, t_{esc}, on the number of hydrophobic residues, N_h, and the total charge, Q, for all the considered proteins at the T3 tunnel model (the values of t_{esc} are listed in Table 1, whereas N_h and Q can be found in Table S1). We find that t_{esc} correlates with both N_h (Fig. 6 *A*) and Q (Fig. 6 *B*) with the corresponding Pearson correlation coefficients $R = 0.701$ and $R = 0.928$, respectively. Remarkably, maximizing the correlation between t_{esc} and a combined function $N_h + \alpha Q$ of both N_h and Q with respect to the α-value yields the best correlation of $R = 0.963$ for $\alpha = 5.9$ (Fig. 6 *C*). The

TABLE 1 Escape and folding properties of nascent proteins obtained by simulations for different types of the tunnel model

System	D (Å$^2\tau^{-1}$)	βk (Å^{-1})	$t_{esc}(\tau)$	$t_{fold}(\tau)$
GB1, T1	0.7781	0.3122	282.0	478.9
GB1, T2	0.8974	0.1787	423.8	652.9
GB1, T3	0.8794	0.3410	233.6	395.1
SH3, T1	0.6783	0.3447	295.3	635.9
SH3, T2	0.6790	0.1639	592.0	803.9
SH3, T3	0.5962	0.1377	806.2	1182.1
SpA, T3	0.4465	0.2518	607.0	865.7
CI2, T3	0.9746	0.0763	817.5	1763.5
CSP, T3	0.8331	0.2953	282.2	3531.1
UBQ, T3	0.6328	0.1553	677.2	825.9
Barnase, T3	0.9207	0.0682	954.6	3239.5

For each protein and tunnel type, shown are the diffusion constant (D), the parameter βk of the potential field in the diffusion model, the median escape time (t_{esc}), and the median folding time (t_{fold}). The simulations are carried out at $T = 298$ K with $t_g = 400\tau$.

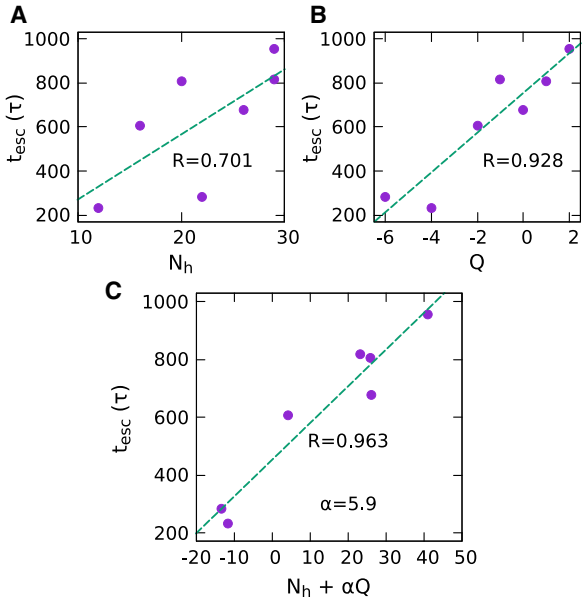

FIGURE 6 Dependence of the median escape time t_{esc} on the number of hydrophobic residues N_h (*A*) and the total charge Q (*B*) with the Pearson correlation coefficients $R = 0.701$ in (*A*) and $R = 0.928$ in (*B*). (*C*) Dependence of the median escape time t_{esc} on a function $(N_h + \alpha Q)$ of the number of hydrophobic residues N_h and the total charge Q. The best correlation of $R = 0.963$ was obtained for $\alpha = 5.9$. The data shown are obtained for the seven considered proteins at the T3 tunnel. To see this figure in color, go online.

obtained correlations indicate that energetic interactions influence the escape time in a predictable way. They show that both the increases of N_h and Q lead to an increase in the escape time, and the escape time appears to depend more strongly on the total charge of a protein than on its number of hydrophobic residues. The optimal α-value suggests that the dependence of t_{esc} on Q is ~6 times stronger than on N_h. Note that $N_h + \alpha Q$ is the simplest function for the assumption of additive effects of hydrophobic and electrostatic interactions on the escape time. The strong correlation obtained for $\alpha = 5.9$ indicates that such function can be considered as first-order approximation of the true dependence of t_{esc} on N_h and Q.

The correlations of t_{esc} with N_h and Q show a simple tendency that the stronger the protein is attracted to the wall of the ribosome tunnel, the more retarded is the escape process. This tendency looks obvious but is not trivial. In fact, the correlations shown in Fig. 6 are not for a single protein but for a bunch of different proteins—the quantitative impacts of the tunnel interactions on the escape time can be different for different proteins. Furthermore, the combined effects of attraction and repulsion, as well as of hydrophobic and electrostatic interactions on the escape time are not easily predicted. Our result gives useful insights to these issues.

It is interesting to check whether the energetic interactions with the ribosome tunnel have any visible impact on

the folding time of nascent proteins because the escape time is part of the folding time at the tunnel. In contrast to the median escape time, the median folding time at the tunnel has little correlation with the number of hydrophobic residues and almost no correlation with the total charge (see Fig. S2). The folding time at the tunnel therefore does not depend explicitly on the tunnel interactions. We have also checked that the median folding time is almost uncorrelated to the median escape time with a correlation coefficient smaller than 0.14.

The median escape times obtained by simulations at the T3 tunnel for the proteins considered vary from 234τ for GB1 to 955τ for barnase. By mapping to real time at realistic friction, they are in the range from 0.07 to 0.3 ms. Given that the predicted timescale in simulations can be 10 times smaller than experiments (see Materials and methods), the escape times of these proteins can be ranged up to 3 ms. It can be projected from the fits in Fig. 6 that for proteins of a much higher positive net charge than barnase, such as $Q = +10e$, the median escape time is longer but should not exceed 10 ms. As discussed, this timescale should not lead to the jamming of the ribosome tunnel. It should be also noted that given the broad distribution of the escape time, some individual escape process may take a much longer time, but the probability of having an escape time larger than the median escape time by several times is vanishingly small.

Diffusion properties

For all proteins and all tunnel types considered, we find that the escape time distribution can be well fitted to the diffusion model (see Fig. 4, *A–C* for GB1, Fig. 5, *A–C* for SH3, and Fig. S1, *A–E* for other proteins). This suggests that the tunnel interactions do not change the diffusion mechanism of the protein escape process, but only its quantitative properties. The latter can be expressed by the diffusion constant D of the protein and the slope βk of the effective potential in the diffusion model. From the values of D and βk obtained by the fits for GB1 and SH3 at the three tunnel types (Table 1), one can find that the tunnel hydrophobic and electrostatic interactions affect βk more strongly, whereas they only mildly affect D. The changes in βk are qualitatively consistent with the effects of attractive and repulsive interactions on the escape time. For example, for protein GB1, by adding the hydrophobic interaction, which is attractive, βk drops from 0.3122 to 0.1787 Å^{-1} on switching from the T1 tunnel to the T2 tunnel. By including the electrostatic interaction, which is overall repulsive for GB1, βk increases from 0.1787 to 0.3410 Å^{-1} on switching from the T2 tunnel to the T3 tunnel. Also note that βk is smallest for barnase and CI2. These two proteins have the highest number of hydrophobic residues (of 29 each), and barnase has the highest total charge (of $+2e$) among the proteins considered; therefore, they also have the strongest attractions to the tunnel. The changes in D, on the other hand, depend on the protein and do not follow the effects of attractive and repulsive interactions. D is found to vary between 0.44 and 0.97 $\text{Å}^2\tau^{-1}$ (Table 1), not as strongly as βk.

Our previous work (23) has shown that D increases linearly with temperature, suggesting that it can be expressed by the Einstein's formula, $D = k_B T/\zeta^*$, where ζ^* is an effective friction coefficient of a protein at the tunnel. ζ^* should depend on the protein size as well as on the protein conformation, therefore, generally, D are different for different proteins. In principle, attraction to the tunnel wall should increase the friction on nascent proteins, leading to a decrease in D. We observe this attraction-induced decrease for SH3 on switching from the T2 to the T3 tunnel but not for GB1 on switching from the T1 to the T2 tunnel (see Table 1). Thus, the changes in the tunnel interactions are not well reflected in the diffusion constant D. This may be due to the fact that the diffusion model assumes a constant D, whereas the latter should change with the protein conformation during the escape process. The slope βk is more sensitive to the tunnel interactions because it is directly related to the protein energy. Note that the values of D in Table 1 with converted units are found in the range from 0.15 to 0.31×10^{-8} m^2 s^{-1}, that is of one to two orders of magnitude larger than the true diffusion constants of isolated proteins in water ($\sim 10^{-10}$ m^2 s^{-1}) (59). This difference is mainly due to the fact that the simulations were run at a low friction of $\zeta = 0.01\zeta_{\text{water}}$. It can be expected that if the simulations were run at the realistic friction, D would have the same order of magnitude but smaller value than the corresponding diffusion constant in water.

The good agreement found between the simulations and the diffusion model suggests that the protein escape process at the ribosome tunnel is akin to a downhill drift in a potential energy landscape without barriers (21). This study shows that this interpretative picture persists for various tunnel models with and without energetic interactions with nascent chains and for various proteins of lengths up to 108 residues. The obtained results indicate that the diffusion model works for any proteins independent of their length. Exceptions may refer only to very short proteins or peptides, such as the zinc-finger domain, which can be severely trapped inside the tunnel (23). For long proteins that fold co-translationally, the escape process is promoted by the folding of the last domain involving the C-terminal fragment.

To understand better the escape process from a thermodynamic viewpoint, we carried out umbrella sampling simulations to calculate the free energy as a function of the number of escaped residues, N_{out}, for protein GB1 at the ribosome tunnel. Fig. 7 shows that the free energy F is approximately a linearly decreasing function of N_{out} for all three types of tunnel model. The linear shape of F indicates that N_{out} is an interesting quantity that reflects the escape coordinate

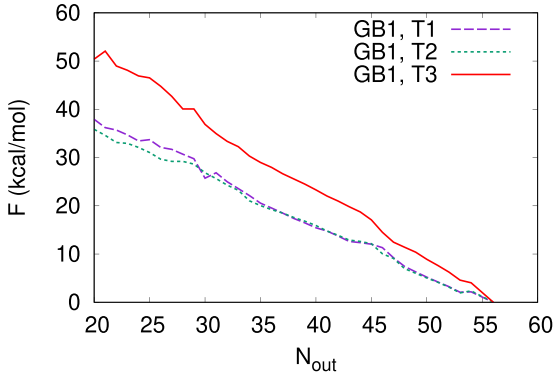

FIGURE 7 Dependence of the free energy F on the number of amino acids escaped from the tunnel (N_{out}) of protein GB1 for the T1 (*dashed*), T2 (*dotted*), and T3 (*solid*) tunnel as indicated. The free energy was calculated at $T = 298$ K based on umbrella sampling simulations with restraint potentials on the protein's C-terminal residue (21). To see this figure in color, go online.

in the diffusion model. Note that the free energy also decreases but not perfectly linearly with the coordinate x_C of the C-terminal residue (see Fig. S3). The relative orders of the mean slopes of F over N_{out} for three tunnel types also qualitatively agree with those obtained for βk: the lowest slope of F corresponds to the T2 tunnel, and the highest slope of F corresponds to the T3 tunnel. The absolute values of the slopes in F, however, are about three to four times higher than those given by βk. Fig. 7 shows that the total free energy differences ΔF between the states of N_{out} equal to 20 and 56 are ~37, 35, and 50 kcal/mol for the T1, T2, and T3 tunnels, respectively. From the values of βk for GB1, the potential energy difference $\Delta U = kL$ of a full escape process in the diffusion model can be calculated, giving $\Delta U \sim 13.5$, 7.7, and 14.7 kcal/mol for the three tunnel models, respectively. We have checked that the escape process does not necessarily follow the reversible pathway associated with the minimal free energy path sampled by equilibrium umbrella sampling with restraint potentials on the protein's C-terminal residue. The escape pathways of an unrestrained protein usually correspond to conformations of higher energies than those of the reversible one. For example, at the T3 tunnel, in unrestrained simulations, the average energy of the just-escaped conformations (with $N_{out} = 56$ for the first time, to our knowledge) is about -126 kcal/mol (corresponding to ~42% of native contacts), whereas in umbrella sampling, the average energy of the escaped conformations is about -176 kcal/mol (~90% of native contacts).

A recent experiment and simulations (60) show that the folding of the I27 domain of titin at the mouth of the ribosomal exit tunnel induces a pulling force on an arrested peptide through a linker, indicating that the free energy of this protein decreases along the escape direction (the pulling force is always positive). This result is consistent with the monotonic shape of the potential $U(x)$ considered in the diffusion model as well as the free energy profile in Fig. 7, except that the calculated force reported in (60) varies with the linker length, whereas in the diffusion model, the force k is constant. This discrepancy may be due to several reasons, such as the effect of the linker, which can absorb different forces depending on the linker's length, and specific properties of titin, which is known to induce a large force upon folding. Importantly, as pointed out in our analysis of the free energy F, the potential $U(x)$ corresponds to the escape pathways of an unrestrained protein, which are generally different from the minimal free energy pathways sampled by tethered or arrested proteins in equilibrium.

CONCLUSIONS

In this study, we have shown that hydrophobic and electrostatic interactions between nascent proteins and the ribosome tunnel have several effects on the protein escape process. First, these energetic interactions may increase the probability of kinetic trapping of protein at the tunnel compared with the excluded volume tunnel, as shown for the GB1 protein. The trapping probability, however, decreases with the growth time per amino acid in protein elongation and can be vanishingly small at realistic translation rates. We also find that the kinetic trapping depends on the protein and is not an issue for most proteins. Second, the hydrophobic and electrostatic interactions modulate the protein escape time in a simple way; that is, attractive interactions slow down the escape process, and repulsive interactions speed it up. As a result, the median escape time is found to correlate with the number of hydrophobic residues and the net charge of a protein. The result also indicates that changing the total charge of a protein by one elementary charge is equivalent to adding or removing ~6 hydrophobic residues for the same effect on the median escape time. This does not imply that the electrostatic interaction has a stronger effect than the hydrophobic interaction because the charges and the hydrophobicity are not in the same units but suggests that it is easier to modulate the escape time by changing the charges. The strong impact of electrostatic interaction on the escape time reported here is in agreement with a recent study of the protein ejection times at the ribosome tunnel of *Escherichia coli* (24), though the latter indicates a wider variation of the escape times. Our study also indicates that the median escape times of globular proteins are in the submillisecond-to-millisecond range; thus, the escape does not delay the ribosome recycling. Finally, we have shown that the energetic interactions do not alter the diffusional mechanism of the protein escape process. The remarkable consistency between simulations and the diffusion model for various types of tunnel model with different interactions and for various proteins indicate that the protein escape process is governed mainly by the geometry of the tunnel, whereas the tunnel interactions make only the fine

tunings. The consistency with the diffusion model, which describes the escape process as a downhill drift of a Brownian particle, also shows that the escape process is simple and predictable. It seems that such characteristics are necessary for the efficient folding of nascent proteins and for the smooth functioning of ribosomes.

SUPPORTING MATERIAL

Supporting material can be found online at https://doi.org/10.1016/j.bpj.2021.09.027.

AUTHOR CONTRIBUTIONS

T.X.H. designed the research. P.T.B. and T.X.H. carried out the simulations and analyzed the data. P.T.B. and T.X.H. wrote the article.

ACKNOWLEDGMENTS

This research is funded by Graduate University of Science and Technology of the Vietnam Academy of Science & Technology under grant number GUST.STS.DT2020-VL03 for the postdoctoral fellowship of Phuong Thuy Bui and by Vietnam National Foundation for Science and Technology Development under grant number 103.01-2019.363.

REFERENCES

1. Berisio, R., F. Schluenzen, …, A. Yonath. 2003. Structural insight into the role of the ribosomal tunnel in cellular regulation. *Nat. Struct. Biol.* 10:366–370.
2. Nakatogawa, H., and K. Ito. 2002. The ribosomal exit tunnel functions as a discriminating gate. *Cell.* 108:629–636.
3. Nakatogawa, H., and K. Ito. 2004. Intraribosomal regulation of expression and fate of proteins. *ChemBioChem.* 5:48–51.
4. Lu, J., and C. Deutsch. 2008. Electrostatics in the ribosomal tunnel modulate chain elongation rates. *J. Mol. Biol.* 384:73–86.
5. Fedyukina, D. V., and S. Cavagnero. 2011. Protein folding at the exit tunnel. *Annu. Rev. Biophys.* 40:337–359.
6. Fedorov, A. N., and T. O. Baldwin. 1997. Cotranslational protein folding. *J. Biol. Chem.* 272:32715–32718.
7. Javed, A., J. Christodoulou, …, E. V. Orlova. 2017. The ribosome and its role in protein folding: looking through a magnifying glass. *Acta Crystallogr. D Struct. Biol.* 73:509–521.
8. Thommen, M., W. Holtkamp, and M. V. Rodnina. 2017. Co-translational protein folding: progress and methods. *Curr. Opin. Struct. Biol.* 42:83–89.
9. O'Brien, E. P., S.-T. D. Hsu, …, C. M. Dobson. 2010. Transient tertiary structure formation within the ribosome exit port. *J. Am. Chem. Soc.* 132:16928–16937.
10. Holtkamp, W., G. Kokic, …, M. V. Rodnina. 2015. Cotranslational protein folding on the ribosome monitored in real time. *Science.* 350:1104–1107.
11. Nilsson, O. B., R. Hedman, …, G. von Heijne. 2015. Cotranslational protein folding inside the ribosome exit tunnel. *Cell Rep.* 12:1533–1540.
12. Kirmizialtin, S., V. Ganesan, and D. E. Makarov. 2004. Translocation of a β-hairpin-forming peptide through a cylindrical tunnel. *J. Chem. Phys.* 121:10268–10277.
13. Lu, J., and C. Deutsch. 2005. Folding zones inside the ribosomal exit tunnel. *Nat. Struct. Mol. Biol.* 12:1123–1129.
14. Kosolapov, A., and C. Deutsch. 2009. Tertiary interactions within the ribosomal exit tunnel. *Nat. Struct. Mol. Biol.* 16:405–411.
15. Voss, N. R., M. Gerstein, …, P. B. Moore. 2006. The geometry of the ribosomal polypeptide exit tunnel. *J. Mol. Biol.* 360:893–906.
16. Marenduzzo, D., T. X. Hoang, …, A. Maritan. 2005. Form of growing strings. *Phys. Rev. Lett.* 95:098103.
17. Siller, E., D. C. DeZwaan, …, J. M. Barral. 2010. Slowing bacterial translation speed enhances eukaryotic protein folding efficiency. *J. Mol. Biol.* 396:1310–1318.
18. Zhang, G., M. Hubalewska, and Z. Ignatova. 2009. Transient ribosomal attenuation coordinates protein synthesis and co-translational folding. *Nat. Struct. Mol. Biol.* 16:274–280.
19. O'Brien, E. P., M. Vendruscolo, and C. M. Dobson. 2014. Kinetic modelling indicates that fast-translating codons can coordinate cotranslational protein folding by avoiding misfolded intermediates. *Nat. Commun.* 5:2988.
20. Tanaka, T., N. Hori, and S. Takada. 2015. How co-translational folding of multi-domain protein is affected by elongation schedule: molecular simulations. *PLoS Comput. Biol.* 11:e1004356.
21. Bui, P. T., and T. X. Hoang. 2016. Folding and escape of nascent proteins at ribosomal exit tunnel. *J. Chem. Phys.* 144:095102.
22. Bui, P. T., and T. X. Hoang. 2018. Protein escape at the ribosomal exit tunnel: effects of native interactions, tunnel length, and macromolecular crowding. *J. Chem. Phys.* 149:045102.
23. Bui, P. T., and T. X. Hoang. 2020. Protein escape at the ribosomal exit tunnel: effect of the tunnel shape. *J. Chem. Phys.* 153:045105.
24. Nissley, D. A., Q. V. Vu, …, E. P. O'Brien. 2020. Electrostatic interactions govern extreme nascent protein ejection times from ribosomes and can delay ribosome recycling. *J. Am. Chem. Soc.* 142:6103–6110.
25. Lucent, D., C. D. Snow, …, V. S. Pande. 2010. Non-bulk-like solvent behavior in the ribosome exit tunnel. *PLoS Comput. Biol.* 6:e1000963.
26. Vu, Q. V., Y. Jiang, …, E. O'Brien. 2021. The driving force for co-translational protein folding is weaker in the ribosome vestibule due to greater water ordering. *Chem. Sci. (Camb.).* 12:11851–11857.
27. Dao Duc, K., S. S. Batra, …, Y. S. Song. 2019. Differences in the path to exit the ribosome across the three domains of life. *Nucleic Acids Res.* 47:4198–4210.
28. Lu, J., W. R. Kobertz, and C. Deutsch. 2007. Mapping the electrostatic potential within the ribosomal exit tunnel. *J. Mol. Biol.* 371:1378–1391.
29. Liao, S., J. Lin, …, A. E. Johnson. 1997. Both lumenal and cytosolic gating of the aqueous ER translocon pore are regulated from inside the ribosome during membrane protein integration. *Cell.* 90:31–41.
30. Clementi, C., H. Nymeyer, and J. N. Onuchic. 2000. Topological and energetic factors: what determines the structural details of the transition state ensemble and "en-route" intermediates for protein folding? An investigation for small globular proteins. *J. Mol. Biol.* 298:937–953.
31. Onuchic, J. N., N. D. Socci, …, P. G. Wolynes. 1996. Protein folding funnels: the nature of the transition state ensemble. *Fold. Des.* 1:441–450.
32. Baker, D. 2000. A surprising simplicity to protein folding. *Nature.* 405:39–42.
33. Hoang, T. X., and M. Cieplak. 2000. Sequencing of folding events in Go-type proteins. *J. Chem. Phys.* 113:8319–8328.
34. Hills, R. D., Jr., and C. L. Brooks, III. 2009. Insights from coarse-grained Gō models for protein folding and dynamics. *Int. J. Mol. Sci.* 10:889–905.
35. Takada, S. 2019. Gō model revisited. *Biophys. Physicobiol.* 16:248–255.
36. Karanicolas, J., and C. L. Brooks, III. 2003. Improved Gō-like models demonstrate the robustness of protein folding mechanisms towards non-native interactions. *J. Mol. Biol.* 334:309–325.
37. Alexander, P., J. Orban, and P. Bryan. 1992. Kinetic analysis of folding and unfolding the 56 amino acid IgG-binding domain of streptococcal protein G. *Biochemistry.* 31:7243–7248.

38. Chen, Y.-J., S.-C. Lin, …, J.-W. Cheng. 1996. Stability and folding of the SH3 domain of Bruton's tyrosine kinase. *Proteins.* 26:465–471.

39. Myrhammar, A., D. Rosik, and A. E. Karlström. 2020. Photocontrolled reversible binding between the protein A-derived Z domain and immunoglobulin G. *Bioconjug. Chem.* 31:622–630.

40. Jackson, S. E., and A. R. Fersht. 1991. Folding of chymotrypsin inhibitor 2. 1. Evidence for a two-state transition. *Biochemistry.* 30:10428–10435.

41. Welte, H., T. Zhou, …, M. Kovermann. 2020. What does fluorine do to a protein? Thermodynamic, and highly-resolved structural insights into fluorine-labelled variants of the cold shock protein. *Sci. Rep.* 10:2640.

42. Morimoto, D., E. Walinda, …, M. Shirakawa. 2015. The unexpected role of polyubiquitin chains in the formation of fibrillar aggregates. *Nat. Commun.* 6:6116.

43. Bye, J. W., N. J. Baxter, …, M. P. Williamson. 2016. Molecular mechanism for the Hofmeister effect derived from NMR and DSC measurements on barnase. *ACS Omega.* 1:669–679.

44. Taketomi, H., Y. Ueda, and N. Gō. 1975. Studies on protein folding, unfolding and fluctuations by computer simulation. I. The effect of specific amino acid sequence represented by specific inter-unit interactions. *Int. J. Pept. Protein Res.* 7:445–459.

45. Tsai, J., R. Taylor, …, M. Gerstein. 1999. The packing density in proteins: standard radii and volumes. *J. Mol. Biol.* 290:253–266.

46. Cieplak, M., and T. X. Hoang. 2002. The range of the contact interactions and the kinetics of the Go models of proteins. *Int. J. Mod. Phys. C.* 13:1231–1242.

47. Ferrenberg, A. M., and R. H. Swendsen. 1989. Optimized Monte Carlo data analysis. *Phys. Rev. Lett.* 63:1195–1198.

48. Kumar, S., J. M. Rosenberg, …, P. A. Kollman. 1992. The weighted histogram analysis method for free-energy calculations on biomolecules. I. The method. *J. Comput. Chem.* 13:1011–1021.

49. Ban, N., P. Nissen, …, T. A. Steitz. 2000. The complete atomic structure of the large ribosomal subunit at 2.4 A resolution. *Science.* 289:905–920.

50. Kellis, J. T., Jr., K. Nyberg, …, A. R. Fersht. 1988. Contribution of hydrophobic interactions to protein stability. *Nature.* 333:784–786.

51. Pace, C. N., H. Fu, …, G. R. Grimsley. 2011. Contribution of hydrophobic interactions to protein stability. *J. Mol. Biol.* 408:514–528.

52. Germann, M. W., T. Turner, and S. A. Allison. 2007. Translational diffusion constants of the amino acids: measurement by NMR and their use in modeling the transport of peptides. *J. Phys. Chem. A.* 111:1452–1455.

53. Hoang, T. X., and M. Cieplak. 2000. Molecular dynamics of folding of secondary structures in Go-type models of proteins. *J. Chem. Phys.* 112:6851–6862.

54. Klimov, D. K., and D. Thirumalai. 1997. Viscosity dependence of the folding rates of proteins. *Phys. Rev. Lett.* 79:317–320.

55. Veitshans, T., D. Klimov, and D. Thirumalai. 1997. Protein folding kinetics: timescales, pathways and energy landscapes in terms of sequence-dependent properties. *Fold. Des.* 2:1–22.

56. Torrie, G. M., and J. P. Valleau. 1977. Nonphysical sampling distributions in Monte Carlo free-energy estimation: umbrella sampling. *J. Chem. Phys.* 23:187–199.

57. Van Kampen, N. G. 1992. Stochastic Processes in Physics and Chemistry, Third Edition. Elsevier, Amsterdam.

58. Cox, D. R., and H. D. Miller. 1965. The Theory of Stochastic Processes. Chapman and Hall, London.

59. Brune, D., and S. Kim. 1993. Predicting protein diffusion coefficients. *Proc. Natl. Acad. Sci. USA.* 90:3835–3839.

60. Tian, P., A. Steward, …, R. B. Best. 2018. Folding pathway of an Ig domain is conserved on and off the ribosome. *Proc. Natl. Acad. Sci. USA.* 115:E11284–E11293.